9

Precision Timekeeping: Optical Atomic Clocks

Shimon Kolkowitz and Jun Ye

CONTENTS

9.1 Principles of Atomic Clocks

Clocks are the metrological tools used to measure the passage of time in seconds, the SI unit for time. All precise clocks do this by counting the cycles of a periodic physical phenomenon, such as the oscillations of a pendulum, as in a grandfather clock, or the vibrations of a piezoelectric tuning fork, as used in modern electronics. Because these periods ideally occur regularly, the number of counted periods is a measure of the amount of time that has passed. However, because no two man-made oscillators are ever identical, and because the frequency of their oscillations is coupled to their changing external environments, two oscillators will inevitably drift away from each other, limiting their stability, and both oscillators will always have a finite error relative to the agreed upon standard definition of the second, limiting their accuracy.

In contrast, all atoms of the same elemental and isotopic species are indistinguishable. Atomic clocks take advantage of this to achieve greater levels of both stability and

accuracy by referencing the oscillations of a man-made "local oscillator," such as a piezoelectric tuning fork or the electro-magnetic modes of a microwave or optical cavity, to the resonance frequency of a "clock transition" between two internal energy levels in an atom of choice. This also enables the definition of the SI second with respect to the frequency of this transition, a constant of nature that, at least as far as we know, is the same in every inertial frame of reference (a principle that is foundational to the theories of both special and general relativity).

However, whilst two atoms placed in identical conditions will have the same internal structure, their energy levels can be shifted with respect to each other by external perturbations such as electric and magnetic fields. The achievable accuracy and stability of a particular atomic clock is therefore determined by three related factors: (i) how well the effects of external perturbations on the energy levels of the two clock states are understood, limiting accuracy; (ii) how precisely and rapidly deviations in frequency between the local oscillator and the atomic frequency reference can be measured and corrected, limiting stability; and (iii) how well the external environment can be measured and controlled, which limits the reproducibility of the clock, and therefore both its accuracy and long-term stability. In the following subsections, we elaborate on these factors and their roles in clock performance, including the relevant figures of merit.

9.1.1 Clock Stability

The fractional frequency instability (often simply called the stability) of a clock, $\sigma_y(\tau)$, is a unitless number that parameterizes how precisely deviations in frequency between the local oscillator and the atomic frequency reference can be measured and corrected over a measurement of total duration τ. The smaller $\sigma_y(\tau)$, the more stable, or precise, the clock. One way to think about the stability of a clock is as the consistency with which the clock keeps time over some period of time. As a simple example, consider two clocks, A and B, both of which nominally oscillate at 1 GHz. We assume that clock B is much more stable than clock A and can therefore serve as a reference clock. If over the course of many comparisons of duration 1 s clock A is measured to have a standard deviation in frequency of 5 Hz with respect to clock B, then the stability of clock A is $\sigma_y(1\,\mathrm{s}) = 5\ \mathrm{Hz}/1\ \mathrm{GHz} = 5\times10^{-9}$. If clock A was then used to keep time, over the course of 1 s on average it would lose or gain ±5 nanoseconds. This simple example highlights the difficulty in determining the stability of a very stable clock, in that it can only be measured through comparisons with other clocks of comparable stability.

At short timescales (on the order of seconds to hours) $\sigma_y(\tau)$ is typically limited by noise that obscures the measurement of the offset of the local oscillator frequency from the frequency of the atomic reference. Therefore, the less noisy the local oscillator and the atoms are, the smaller $\sigma_y(\tau)$ will be and the more consistently the clock will keep time from second to second. Often the noise at these timescales has a flat frequency spectrum and therefore can be averaged down. The stability of an atomic clock therefore typically improves with averaging time τ for hours of measurement.

We now consider the stability of an atomic clock more quantitatively. As described in the previous section and shown in Figure 9.1, an optical atomic clock operates by locking the frequency of a drifting local oscillator to that of a narrow atomic transition. This is typically done by preparing N atoms into the ground clock state $|g\rangle$ and then driving the atoms with radiation at the frequency of the local oscillator and measuring the subsequent atomic populations $N_{g,e}$ in states $|g\rangle$ and $|e\rangle$ using a strong optical cycling transition (Nagourney et al. 1986), which enables high-fidelity projective single-shot measurement of each atom's state. With a judicious choice of measurement sequence, driving strength, and detuning (see Section 9.3.1), the excitation fraction $P_e = N_e/(N_e+N_g)$ will be linearly proportional to the detuning from resonance Δ and can be used as a discriminator signal to feed back on the local oscillator and keep it locked to the atomic reference. The statistical errors in the measurement of Δ introduced by a combination of fundamental and technical noise sources will limit the stability $\sigma_y(\tau)$ of the clock.

The measurement of P_e, and therefore of Δ, is fundamentally limited by the quantum noise associated with the projective measurement of each atom's state into either $|g\rangle$ and $|e\rangle$. In the absence of any other sources of noise and for a clock interrogation time of length T with no dead time between measurements, the clock stability will be given by

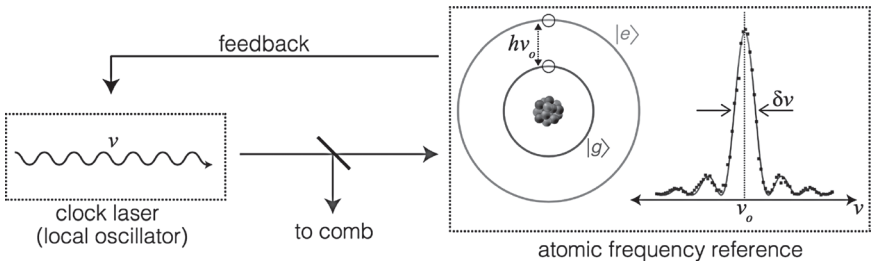

FIGURE 9.1 Diagram of optical atomic clock operation. In an optical atomic clock, a stable laser at frequency ν serves as the local oscillator. It is used to interrogate atoms prepared in the ground state $|g\rangle$ of an ultra-narrow optical atomic transition whose frequency ν_o and linewidth $\delta\nu$ serve as the frequency reference. The number of atoms in the excited state $|e\rangle$ after the clock interrogation is used to feed back on the clock laser frequency and stabilize it at or near $\nu = \nu_o$. The frequency-stabilized clock laser is sent to an optical frequency comb, which is used to convert the optical frequency either to a microwave clock signal or to another optical frequency. The data were taken with a strontium optical lattice clock in the Ye group at JILA and is an example of Rabi spectroscopy of an optical clock transition (see Section 9.3.1).

$$\sigma_y(\tau) = \frac{1}{2\pi\nu_0 T}\sqrt{\frac{T}{N\tau}}, \tag{9.1}$$

where ν_o is the frequency of the transition and N is the number of atoms in the clock (Campbell et al. 2017). This equation is quite easy to understand. The first term is the inverse number of frequency reference cycles that are counted in a single measurement (in inverse radians). The more cycles that can be counted in a single measurement, the more information is gained about the relative detuning of the oscillator from the frequency reference. The second term is the square root of the inverse total number of single atom measurements performed in time τ, which can be interpreted as the improvement of signal-to-noise ratio with more averages. From this equation, we can see that for a quantum projection noise-limited atomic clock, the stability will improve with increasing averaging time, scaling with $\tau^{-1/2}$.

Equation (9.1) offers a number of insights into the design of the ideal atomic clock. First, the scaling with $1/\sqrt{N}$ indicates that interrogating a large number of atoms simultaneously is advantageous. Second, the overall factor of $\sqrt{T}$ in the denominator indicates that a long-lived atomic transition is desirable, as the lifetime of the transition imposes an ultimate limit on the length of a single-clock measurement. Fortunately, a number of candidate atoms exhibit appropriately named "clock transitions" which are highly insensitive to external perturbations and are very long lived. To take full advantage of these transitions, a local oscillator with as long of a coherence time as possible should also be used. However, the interrogation time can also be limited by other sources of dephasing. The atoms should therefore be well isolated from their surrounding environment and from interactions with each other to reduce inhomogeneous broadening of the atomic transition, and should be as cold as possible to reduce Doppler broadening. As the temperature limits of laser cooling are insufficient to narrow the Doppler linewidth down to the natural linewidths of optical clock transitions, the atoms should be trapped in a confining potential to further decouple the clock transition from the finite atomic temperature, and to increase the interrogation time T to the transition lifetime $T_e = 1/2\pi\delta\nu$, where $\delta\nu$ is the clock transition linewidth (Ludlow et al. 2015, Poli et al. 2014).

Finally, and perhaps most importantly in the context of this chapter, the factor of ν_o in the denominator explains the advantage of moving from microwave atomic clocks, with transition frequencies of $\nu_o \approx 10^{10}$ Hz, to optical atomic clocks, with frequencies of $\nu_o \approx 10^{15}$ Hz. This can intuitively be understood as the advantage of counting seconds instead of counting days when trying to accurately measure the passage of time (Diddams et al. 2004). Simply put, the more cycles that can be counted in a single measurement, the better the measurement will be. All other factors remaining equal, the use of optical frequency transitions offers orders of magnitude gains in clock stability. Of course, this is much easier said than done. At present there are no electronics fast enough to count the oscillations of optical frequency electromagnetic radiation, so it was not until the start of the 21st century and the advent of the optical frequency comb, which enables the transfer of stability from an optical local oscillator to the microwave domain (see Section 9.2.2), that optical clocks became a practical reality.

As the measurement and local oscillator noise are averaged down, at longer timescales (typically on the order of hours to days), $\sigma_y(\tau)$ can become limited by uncontrolled low-frequency fluctuations of the surrounding environment, and equation (9.1) will no longer be valid. This results in slowly varying systematic shifts that limit the reproducibility of the clock frequency measurement, and at these time scales $\sigma_y(\tau)$ will either bottom out or even begin to grow with τ (Ludlow et al. 2015, Poli et al. 2014). Of course, the reproducibility of the clock frequency represents a limit not only on the day-to-day stability of a clock but also on the level of agreement it can be expected to have with a different clock or with the accepted definition of the second, which is parameterized by the clock accuracy.

9.1.2 Clock Accuracy

In addition to the statistical errors described in Section 9.1.1, the accuracy of an atomic clock is limited by systematic errors associated with shifts of the atomic clock transition frequency due to the surrounding environment. The extent to which systematic shifts can be anticipated, characterized, and controlled determines the level of accuracy at which the true frequency of the atomic transition can be determined and, therefore, the level of agreement that can be expected between the frequencies of two different clocks at long measurement times (Ludlow et al. 2015, Poli et al. 2014).

While the frequency of a particular atomic transition is a constant of nature, it is not a fundamental constant, and we do not presently have the tools to predict the frequency of a particular clock transition to anywhere near the accuracy with which we can measure it. The goal is therefore to anticipate, evaluate, and control all possible systematic shifts of a clock-transition frequency through a combination of theory and experiment, and to then verify the consistency of these evaluations through comparisons between clocks. Because the accuracy of optical clocks now exceeds the fractional precision with which the SI second is defined (Ludlow et al. 2015), optical clock comparisons now consist of precise measurements of the frequency ratios between optical transitions, which are absolute constants that are independent of unit definitions, and can be measured at the level of precision set by the constituent clocks.

Common sources of systematic shifts of clock transition frequencies include electric and magnetic fields, interactions between atoms, and motion of the atoms with respect to the lab frame which results in Doppler shifts of the atomic transition frequency. In addition, relative motion and differences in altitude on Earth will result in relativistic shifts that will appear in comparisons between clocks. It is not always necessary or even desirable to eliminate such shifts, but it is critical that they be known to the desired level of accuracy and included in an overall accounting of all the systematic effects. In Section 9.3.2 we summarize some of the major systematics for optical clocks. However, the dominant systematics can vary considerably for each atomic species and experimental apparatus, and we briefly discuss some of the systematics that are specific to ion and lattice clocks in Sections 9.3.3 and 9.3.4, respectively. In addition, as clock accuracy continues to improve through better understanding and control of the

current limiting systematic effects, previously insignificant or unforeseen effects will undoubtedly emerge. While this represents a challenge to developing ever more accurate clocks, it also represents an opportunity, as many of these effects are interesting and worthy of study in their own right, as we discuss in Section 9.4.2.

Despite the distinctions we have drawn between accuracy and stability, they remain intimately connected. As discussed in Section 9.1.1, if the environment is not well controlled and the systematic shifts drift with time the reproducibility of the clock will be limited, and the long-term stability may be worse than the short-term stability, as with hydrogen masers or quartz oscillators. Similarly, the stability of a clock often determines how quickly a particular systematic shift can be evaluated through averaging. As a result, clock stability and accuracy have historically progressed hand in hand.

9.2 Ultra-stable Optical Cavities and Optical Frequency Combs

9.2.1 Ultra-stable Optical Cavities

In an optical atomic clock the local oscillator must oscillate at an optical frequency resonant with the atomic transition, which naturally suggests the use of a laser. However, as discussed in Section 9.1.1, in order to achieve high levels of clock stability the local oscillator should have a linewidth comparable to the ~ 1 – 1000 mHz atomic clock transition linewidth, whilst free-running lasers typically have linewidths many orders of magnitude broader than this. Furthermore, in current optical clocks noise on the clock laser is actually even more detrimental due to the "Dick effect," in which the finite dead time required to cool and reload atoms in each measurement cycle leads to laser-noise-limited clock stabilities well above the quantum projection noise limit given by equation (9.1). The Dick effect can be understood as an aliasing down of higher frequency laser noise due to the stroboscopic measurements with the atoms (Santarelli et al. 1998, Westergaard et al. 2010) and is currently the limiting factor for optical lattice clock stabilities (Schioppo et al. 2017). The desire to improve achievable clock stabilities has therefore motivated a concerted research effort into the generation of ultra-stable laser light.

While novel techniques for laser stabilization such as spectral hole burning in rare earth-doped crystals and hybrid atom-cavity geometries are currently being explored (Cook et al. 2015, Christensen et al. 2015), so far the most successful and widely adopted laser stabilization technique is to lock the laser to a passive, ultra-stable, high-finesse, two-mirror optical cavity (Matei et al. 2017) using the Pound-Drever-Hall locking technique (Drever et al. 1983), which is described in Chapter [Laser Stabilization for Precision Measurements]. The linewidth of the laser is then determined by the stability of the cavity resonance frequency, which in turn depends on the cavity length. To stabilize the cavity length, the two mirrors are mounted on either end of a transparent, solid spacer. The spacer is shaped and mounted to minimize length changes due to accelerations of the cavity from acoustic and mechanical vibrations of the surrounding environment (Swallows et al. 2012, Nazarova et al. 2006, Millo et al. 2009). The spacer material is selected to have a low coefficient of thermal expansion at the operating temperature, and the cavity is kept in a temperature-stabilized, thermally shielded vacuum chamber. The end result is that the frequency stability of these cavities at relevant clock interrogation times is no longer limited by their coupling to the outside environment, but rather by the thermal fluctuations of the spacer material and mirror coatings (Bishof et al. 2013, Ludlow et al. 2007, Webster et al. 2008, Jiang et al. 2011). These thermal fluctuations can be reduced by moving to cryogenic temperatures in vibration-isolated cryostats and by using cavities with rigid single-crystal spacers (Kessler et al. 2012), Matei et al. 2017), Zhang et al. 2017)) and crystalline mirror coatings (Cole et al. 2013). These efforts have recently culminated in the demonstration of sub-10 mHz laser linewidths and corresponding laser stabilities of $\sigma_y = 4\times10^{-17}$ at 1 s (Matei et al. 2017), as shown in Figure 9.2.

9.2.2 Optical Frequency Combs

The ultra-stable optical cavities described in Section 9.2.1, combined with the techniques for stabilizing an optical local oscillator to a narrow optical clock transition described in Section 9.3, enable the generation of remarkably stable lasers with a known absolute frequency relative to the natural atomic transition. However, the utility of this laser would be quite limited without the ability to compare it to other optical frequencies or to reference its frequency down to the microwave regime so that it can be counted by modern electronics and compared to microwave atomic frequency standards. Fortunately, this is made possible by the optical frequency comb.

To understand how a frequency comb can be used to transfer the stability of an optical-clock-stabilized local oscillator at frequency f_L down to microwave frequencies, consider a mode-locked laser (see Chapter [Mode-Locked Lasers] for details) with a repetition rate of f_{rep} (typically ~100–1000 MHz), and a carrier-envelope offset frequency f_0 as shown in Figure 9.3. The nth comb tooth will have a frequency given by $f_n = f_0 + nf_{\text{rep}}$. When the mode-locked laser is free running, f_0 can take any value between $0 - f_{\text{rep}}$ and will drift over time. However, if the mode-locked laser is sent through a non-linear optical element such as a photonic crystal fibre to generate a harmonic spanning spectrum, f_0 can be stabilized using a $f - 2f$ interferometer. The nth comb tooth is frequency-doubled using second-harmonic generation and interfered with the $2n$th comb tooth at frequency f_{2n}, to produce a beat note at $2f_n - f_{2n} = 2\left(f_0 + nf_{\text{rep}}\right) - \left(f_0 + 2nf_{\text{rep}}\right) = f_0$, which can then be stabilized to a microwave reference, such as a GPS-trained 10 MHz oscillator or a caesium or rubidium vapour cell clock.

If an optical clock laser is then interfered with the mth comb tooth with frequency f_m it will produce a beat note at $f_m - f_L = f_0 + mf_{\text{rep}} - f_L$. This beat note can then be stabilized by feeding back on f_{rep}, such that the microwave frequency f_{rep} now has the stability of the stabilized clock laser. While the frequency f_{rep} will also depend on f_0, its contribution is divided down by a factor of m where $m \approx 10^{14}\,\text{Hz}/100\,\text{MHz} = 1\times10^6$. As a result the stability of the microwave standard is divided down by a large enough factor to make its contribution

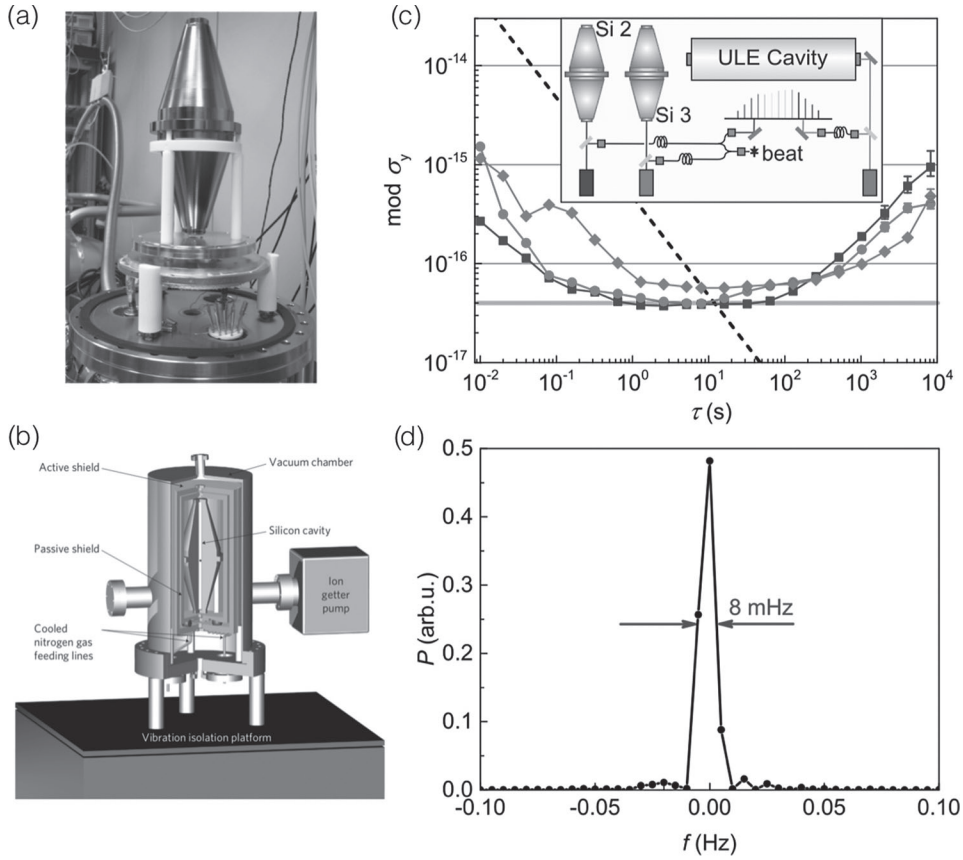

FIGURE 9.2 Ultra-stable optical cavities. (a) One of the two single-crystal silicon optical cavities from the JILA-PTB ultra-stable cavity collaboration, which has been machined and mounted to minimize susceptibility to accelerations. (b) Schematic of the single-crystal silicon cavity (a) in a nitrogen-gas-based vibration-isolated cryostat, including the vacuum chamber and two heat shields. Figure published in Kessler et al. (2012). (c) A comparison between the two cryogenic single-crystal silicon optical cavities and a ULE cavity, demonstrating silicon cavity stabilities of $\sigma_y = 4\times10^{-17}$ at 1 s. Data and figure published in Matei et al. (2017). (d) A measured sub-10 mHz linewidth beat note between the two single-crystal silicon optical cavities. (Data and figure published in Matei et al. 2017.)

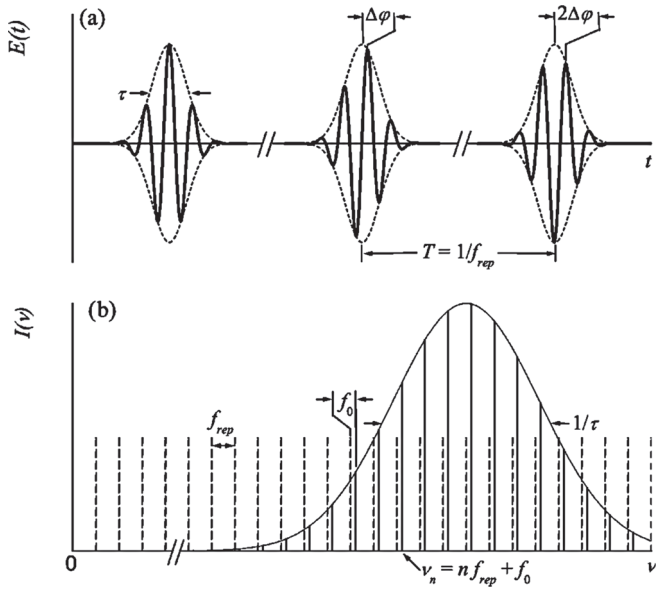

FIGURE 9.3 The optical frequency comb. (a) In the time domain, a frequency comb consists of a train of periodically spaced femtosecond laser pulses with well-defined carrier phase relationships between each pulse. (b) In the frequency domain, this corresponds to a broad spectrum of equally spaced, sharp "comb teeth." The frequency of each tooth is uniquely determined by f_{rep} and the phase offset between subsequent pulses $\Delta\phi$, which is related to f_0 by $2\pi f_0 = f_{\text{ref}}\Delta\phi$. (Figure from Cundiff & Ye 2003.)

negligible, and the result is a microwave oscillator referenced to the frequency of the clock transition, and with the same fractional frequency stability as the clock laser itself.

With the frequency comb serving as the bridge, optical clocks can be used as ultra-stable microwave frequency references, and the frequency of optical atomic transitions can be measured relative to the current SI unit definition of the second based on the caesium hyperfine transition (Udem et al. 2001, Hoyt et al. 2005, Stenger et al. 2001, Margolis et al. 2003, Campbell et al. 2008). Furthermore, the broad spectral span of the comb teeth enables direct frequency ratio comparisons between optical clocks that make use of atomic clock transitions at different optical frequencies (Rosenband et al. 2008, Yamanaka et al. 2015, Nemitz et al. 2016).

9.3 Optical Atomic Clocks

In order to achieve high levels of stability, optical clocks rely on atoms with narrow linewidth optical transitions to maximize the number of cycles in a single measurement, corresponding to minimizing $1/\nu_o T$ in equation (9.1). These are typically either forbidden optical quadrupole transitions in alkali-like ions, or narrow inter-combination transitions in alkaline earth and alkaline-earth-like atoms and ions. Each particular species has its own set of advantages and disadvantages, including the clock transition linewidth, susceptibility to systematic shifts, and the existence and convenience of transitions for laser cooling, state preparation, and optical state read-out.

As one example, in alkaline-earth(-like) atoms, the doubly forbidden $^1S_0$ to $^3P_0$ transition is weakly allowed by hyperfine state mixing in fermionic isotopes with non-zero nuclear spin but is completely forbidden in bosonic isotopes with no nuclear spin. Optical clocks that make use of the bosonic isotopes therefore must artificially introduce state mixing by applying strong magnetic fields or driving additional transitions out of the clock states, which introduce additional systematic shifts. Optical clocks that make use of the fermionic isotopes can avoid these additional environmental perturbations, but the additional hyperfine states make laser cooling more complex and also contribute additional complexity to the evaluation of ac Stark shifts through their coupling to optical polarization (see Section 9.3.4.2).

In addition to the variety of atomic species and transitions to choose from, there are presently also two different leading realizations of optical atomic clocks: single ion clocks and optical lattice clocks. In both cases, the atoms/ions are tightly confined in a trapping potential to isolate the internal clock transition from the motional degrees of freedom. In the following subsections, we describe some of the measurement sequences and systematic shifts that are common to both kinds of optical clock. We then discuss some of the experimental protocols, techniques, and systematics that are specific to each approach.

9.3.1 Clock Interrogation Sequences

To lock the frequency of an ultra-stable clock laser to a narrow atomic clock transition in either an ion or optical lattice clock an appropriate pulse sequence must be applied to convert the resulting clock state population into a discriminator for the detuning of the clock laser from resonance. For this a Ramsey or Rabi spectroscopy sequence can be employed. To understand these sequences, we restrict ourselves to a two-level system defined by the two-clock states, which we label $|g\rangle$ and $|e\rangle$ for the ground and excited states, respectively. Both sequences begin with the atoms prepared in $|g\rangle$.

In the case of the Rabi spectroscopy sequence a single pulse of the clock laser light of length $T_{\text{Rabi}} = \pi/\Omega$ is applied to the atoms, where Ω is the Rabi frequency of the clock light. This is known as a π-pulse, meaning that if the clock laser is exactly on resonance with the atomic transition the atoms will be undergo π radians of a Rabi cycle, and following the pulse all of the atoms will have been coherently transferred to the $|e\rangle$ state. If the detuning of the clock laser from resonance Δ is scanned over the transition and the resulting excited state fraction $P_e(\Delta)$ is measured, the result will be a lineshape of the form $P_e(\Delta) = \frac{\Omega^2}{\Delta^2+\Omega^2}\sin\left(\frac{\pi\sqrt{\Delta^2+\Omega^2}}{2\Omega}\right)^2$ as shown in Figure 9.6c. The clock laser can then be locked to the atomic resonance by fixing the detuning Δ at a point halfway up the slope of the resonance where $P = 0.5$. In the absence of other broadening mechanisms, the width of the Rabi line will be Fourier limited and will scale inversely with T_{Rabi}. Ideally, T_{Rabi} would therefore be set to the lifetime of clock transition; although in practice, it is often limited by the linewidth of the laser, or by other broadening mechanisms.

In the case of Ramsey spectroscopy, the atoms are first driven with a strong $\pi/2$ clock pulse, which places them in a coherent superposition of the two spin states, $|\Psi\rangle = \frac{1}{\sqrt{2}\left(|g\rangle + |e\rangle\right)}$. Left in this state for interrogation time T, the superposition will acquire a relative phase $\phi = \Delta T$, where Δ is the detuning between the laser and the transition angular frequency $\omega_o = 2\pi\nu_o$. With a second strong $\pi/2$ clock pulse at the end of the sequence, the phase ϕ is then converted into a population difference between the two clock states, which can be measured by driving the atoms on a cycling transition out of one of the clock states and collecting the emitted photons. If the Rabi frequency is much larger than the detuning Δ, the fraction of the atoms in $|e\rangle$ at the end of the Ramsey sequence will be given by $P_e = \cos\left(\frac{\Delta T}{2}\right)^2$, and sweeping Δ will produce oscillating Ramsey fringes (as shown in Figure 9.6d), which can be used to generate an error signal and lock Δ to a fixed value. Once again the stability will improve with longer T, and ideally T would correspond to the lifetime of the clock transition. In fact, the clock stability achievable with an ideal Ramsey sequence of length T will be essentially the same as that of an ideal Rabi sequence of length T_{Rabi}. The choice of which sequence to use is therefore dependent on technical considerations specific to each particular clock, such as atomic interaction effects and clock laser ac Stark shifts.

9.3.2 Common Optical Clock Systematic Shifts

The primary systematic effects that are common to both ion and optical lattice clocks are shifts due to electromagnetic fields at the location of the atom, and relativistic shifts arising from atomic motion and gravity. We now briefly discuss each of these effects and the techniques employed to characterize and control them.

9.3.2.1 Magnetic Fields

Static magnetic fields are often intentionally applied to the atoms in an optical clock to define a quantization axis for better internal state control and to lift the degeneracy of hyperfine states in atoms with non-zero nuclear spin. In addition, stray magnetic fields due to the Earth's magnetic field or equipment in the lab may be present at the location of the atoms. The effect of magnetic fields on the clock transition frequency must therefore be accounted for. In general, the ground and excited clock states will have different magnetic moments, and the resulting shift of a particular clock transition in a small magnetic field $\vec{B}$ can be written as an expansion in $\left|\vec{B}\right|$,

$$\Delta\nu_B = C_1\left|\vec{B}\right| + C_2\left|\vec{B}\right|^2 + \cdots, \tag{9.2}$$

where C_i is the ith order magnetic field coupling coefficient for the transition (Ludlow et al. 2015). Typically, only the first two terms need to be considered. Because C_1 is proportional to the angular momentum quantum number m_f, the linear first-order term can either be made zero by using a transition between two clock states with $m_f = 0$ in isotopes with integer angular momentum, or can be cancelled by measuring the transition frequency of two transitions with symmetric shifts, such as between two clock states with $m_f = +9/2$ and between two clock states with $m_f = -9/2$, and averaging them to cancel the shift, as is commonly done in 87Sr optical lattice clocks. The second-order shift can be accounted for by first characterizing C_2 using large magnetic fields and then periodically measuring $\left|\vec{B}\right|$ during clock operation using states with a non-zero C_1.

9.3.2.2 Electric Fields

Electric fields can shift the frequency of the clock transition through the dc Stark and ac Stark effects. While it is unusual to intentionally apply non-zero static electric fields to clock atoms, stray static electric fields may be present due to charge build-up on nearby surfaces. Due to their charge, ions will always move to sit at zero dc electric field, so in ion clocks, there is no dc Stark shift. However, stray electric fields can displace the ion from the null point of the RF fields used to trap the ion, resulting in excess micromotion of the ion and a quadratic Stark shift from the root mean square amplitude of the oscillating-trapping fields.

In contrast to ions, neutral atoms in optical lattice clocks are happy to sit at finite electric fields. The lack of an electric dipole moment in either clock state means that the linear dc Stark shift is negligible, but the second-order quadratic Stark shift arising from stray static electric fields can be significant (Nicholson et al. 2015). The traditional approach in optical lattice clocks has been to carefully characterize and even cancel the dc electric field environment by measuring the Stark shift as additional electric fields are applied via external electrodes (Bloom et al. 2014, Nicholson et al. 2015). This approach has been sufficient to reach dc Stark shift uncertainties at the 10^{-18} level, and recently dc Stark shift uncertainties at the 10^{-20} level were demonstrated in a ytterbium optical lattice clock through a combination of in-vacuum Faraday-shielding and in-vacuum electrodes (Beloy et al. 2018).

Many of the most significant systematics for current optical clocks are ac Stark shift effects from oscillating electric fields. Oscillating electric fields are always present in both ion clocks and optical lattice clocks, due to blackbody radiation (BBR) from the surrounding environment, as well as the clock laser light used to probe the clock transition, which even when on resonance can itself shift the relative energies of the ground and excited clock states due to the existence of other transitions out of both states. In ion traps, there are also the RF fields used to confine the ions, and in the case of quantum logic-based ion clocks (see Section 9.3.3), there are sympathetic cooling lasers. In optical lattice clocks there is also the optical lattice itself, and the frequency and polarization of the lattice must be carefully selected and controlled to minimize the differential ac Stark shift of the clock transition (see Section 9.3.4).

9.3.2.3 Blackbody Radiation

While all of the various ac Stark shifts are important, perhaps the most common limiting systematic for current generation optical clocks is the BBR shift. While the other ac fields are intentionally applied and can be varied to provide a "lever arm" with which to characterize their impact (Bloom et al. 2014), it is difficult to vary the temperature over a large range for room temperature clocks, and the thermal environment is often inhomogeneous and varies with time.

At room temperature the energy density of the BBR spectrum is concentrated at much lower frequencies than the electric dipole-allowed transitions out of the clock states, and so can be approximated as a dc electric field. A higher order "dynamic" correction term is introduced to account for the deviations from this approximation due to the specific transitions out of the clock state that couple most strongly to the blackbody spectrum. The resulting temperature-dependent shift in the clock transition frequency is given by

$$\Delta\nu_{\mathrm{BBR}} = \frac{\Delta\alpha_{\mathrm{s}}\left\langle E^2(T)\right\rangle}{2h}\left(1+\eta\left(T^2\right)\right) \tag{9.3}$$

where $\Delta\alpha_{\mathrm{s}}$ is the differential static scalar polarizability and $\eta(T^2)$ is the dynamic correction term for the clock states, h is Planck's constant, and the temperature dependence of the mean-squared amplitude of the blackbody spectrum can be found by integrating Planck's law, $\left\langle E^2(T)\right\rangle\left(831.9\ \mathrm{V\,m^{-1}}\right)^2\left(T/300\ \mathrm{K}\right)^4$ (Nicholson et al. 2015). The uncertainty in the BBR shift for a specific atomic clock can either come from uncertainty in the effective temperature at the atoms, or in the uncertainty at which $\Delta\alpha_{\mathrm{s}}$ and $\eta(T^2)$, which vary considerably for different

TABLE 9.1

BBR Coefficients for the Clock Transitions in Commonly Used Optical Clock Species, and the Corresponding Frequency Shift and Fractional Frequency Shift at 300 K

Atom/Ion	$\Delta\alpha_s$ (10−41 J m2 V−2)	$\eta(T^2)$	$\Delta\nu_{BBR}$, 300 K (Hz)	$\Delta\nu_{BBR}/\nu_o$, 300 K (10^{-16})
Al+	0.82(8)	$<10^{-4}$	−0.0043	−0.0038
Ca+	−73.0(1.0)		0.380	9.3
Sr+	−47.938(71)	−0.00951(15)	0.248	5.6
Yb+ *E*2	69(14)		−0.36	−5.2
Yb+ *E*3	13(6)		−0.067	−0.97
Hg+	15		−0.079	−1.2
In+	3.3(3)	$<10^{-4}$	−0.017	−0.16
Sr	407.873(11)	0.0698(3)	2.279	−53
Yb	240.269(5)	0.0145(15)	−1.27	−25

Source: All values are taken from Ludlow et al. (2015), other than the values for Sr and Yb which were taken from Nicholson et al. (2015) and Sherman et al. (2012), respectively.

atomic species, is known. In Table 9.1, we list the BBR coefficients for commonly used optical clock species and the corresponding BBR shifts at room temperature.

9.3.2.4 Doppler Shifts

The motion of an atom with respect to the laboratory frame will result in a shift in the measured resonance frequencies of its transitions. An atom moving with velocity $\vec{v}$with respect to a probe laser with wavevector $\vec{k}$, and with a "true" transition frequency ν_o for an atom in its rest frame, will absorb photons from the probe laser at a laser frequency in the lab frame $\nu = \nu_o + \Delta\nu$, where the fractional shift $\Delta\nu/\nu_o$ is given by

$$\frac{\Delta\nu}{\nu_o} \approx \frac{\vec{k}\cdot\vec{v}}{c} - \frac{|\vec{v}|^2}{2c^2} + \frac{|\vec{k}\cdot\vec{v}|^2}{c^2} + O\left(\frac{v}{c}\right)^3, \tag{9.4}$$

where c is the speed of light (Ludlow et al. 2015).

The first term in equation (9.4) is the first-order Doppler shift. For atoms in free space, the first-order Doppler shift results in significant line broadening of their optical transitions due to their Maxwell–Boltzmann velocity distribution. Even for atoms cooled to a temperature of 1 μK, roughly the minimum achievable with laser cooling, the Doppler broadening of an optical transition is tens of kHz. This is the primary reason atoms in an optical clock must be confined. If an atom is confined tightly enough the internal transitions become decoupled from the atomic motion and Doppler broadening can be eliminated (Ido & Katori 2003). However, once the atoms are confined in a trap, a first-order Doppler shift can still arise if the trapping potential itself is moving with respect to the laser, and in ion clocks this must be carefully monitored. In optical lattice clocks this shift can be avoided by referencing the phase of the clock laser to the mirror used to retro-reflect the lattice (Bloom et al. 2014).

The second and third terms in equation (9.4) correspond to the second-order, or relativistic, Doppler shift, which can be interpreted as the special-relativistic time-dilation of the atom's frequency due to its motion with respect to the lab frame. While this effect is small for free-space atoms cooled to μK temperatures (below the 10^{-20} level for the fractional frequency shift of an optical transition), in ion clocks the large trapping frequencies and ion micromotion can result in large velocities even for an ion cooled into the ground state of the trap, and uncertainty in the second-order Doppler shift can be a dominant systematic effect. In optical lattice clocks, the trapping frequencies are low enough that the second-order Doppler shift is not currently relevant.

In addition to the Doppler shifts given in equation (9.4), unconfined atoms will experience an additional "recoil shift" due to the momentum kick an atom receives when it absorbs a photon, given by $\Delta\nu = \hbar k^2/(4\pi m)$, where m is the mass of the atom and k is the wave number of the laser. This shift can be significant for optical transitions, particularly for light atoms, and the resulting motion can result in further complications. The recoil shift therefore provides additional motivation for confining atoms in a trapping potential. For tightly-confined atoms in the "Lamb-Dicke" regime, the momentum kick from the photons is absorbed by the trap, not the atoms, and the recoil shift is strongly suppressed (Ido & Katori 2003).

9.3.2.5 Gravitational Redshift

The theory of general relativity predicts that a difference in gravitational potential between two clocks will result in a gravitational redshift of the relative clock frequencies. On Earth, this means that if one clock is raised with respect to the other, the clock further from the centre of the Earth will appear to tick faster than the lower clock. Expanding the potential to first order, the predicted fractional frequency shift between two clocks for a small height difference Δh and a local acceleration due to gravity $g \approx 9.8\ \mathrm{m\,s^{-2}}$ is given by

$$\frac{\Delta\nu}{\nu_o} \approx \frac{g\Delta h}{c^2}, \tag{9.5}$$

where c is the speed of light (Ludlow et al. 2015). This corresponds to a fractional frequency shift of 1×10^{-18} at a 1-cm height difference. This effect has now been observed at a

height difference of 30 cm using two trapped ion optical clocks (Chou, Hume, Rosenband & Wineland 2010). With clock comparisons now achieving the 10^{-18} level, it has become necessary to measure the relative differences in clock altitude at the mm scale in order to properly account for the gravitational redshift effect, which is pushing the limits of the capabilities of geodetic surveys. While this is problematic for optical clock comparisons, it also presents the opportunity to use optical clocks as a precision tool to measure the Earth's geoid, as discussed in Section 9.4.2. It is worth noting that unlike most other systematics, the gravitational redshift is not a true shift of the clock frequency but rather is a signature of the relative nature of time in a gravitational potential.

9.3.3 Single-Ion Optical Clocks

Ion clocks operate by trapping charged atoms in a harmonic potential at the field minimum of an oscillating RF electric field. Because the ion is extremely well isolated, very tightly confined, and can be cooled to its motional ground state, ion clocks offer narrow clock transition linewidths and excellent control over systematic shifts. Unfortunately, due to the strong Coulomb interaction between ions, at present only one clock ion per harmonic potential is used, limiting the atom number in equation (9.1) to $N = 1$. Nevertheless, single-ion optical clocks with stabilities far surpassing those of microwave atomic clocks and accuracies at the 10^{-18} level have been demonstrated (Huntemann et al. 2016).

9.3.3.1 Ion Clock Operation

Thanks to their charge, ions can be strongly confined using electric fields. Unfortunately, Maxwell's equations forbid the stable trapping of a charged particle in all three dimensions using only dc fields. To circumvent this, in a radio frequency (RF) Paul trap oscillating electric fields are combined with static fields to generate a time-averaged 3D harmonic trapping potential. Figure 9.4 shows some example ion clock Paul trap geometries from the NIST ion clock group in Boulder.

In an ion clock, neutral atoms are produced from a nearby heated source and are then ionized through resonant photoionization. The large trap depths in an RF Paul trap make it possible to then capture single ions in the trap directly, without requiring prior slowing or cooling. Once trapped, a single ion can be held for hours or even months at a time (Ludlow et al. 2015). For clock ions with convenient strong cycling transitions, such as Sr+, Yb+, Ca+, and Hg+, the ion is then laser-cooled using a combination of Doppler cooling and resolved sideband cooling to close to its motional ground state. At this point the ion is ready to be interrogated using one of the clock measurement sequences described in Section 9.3.1. The fluorescent read-out of the clock state population at the end of a clock measurement results in heating of the ion motional state, and the ion must be re-cooled using laser cooling before it can be probed with the clock laser again.

Research into trapped-ion based quantum computation (Leibfried et al. 2003) has led to the development of "quantum logic spectroscopy," which enables the use of ions with

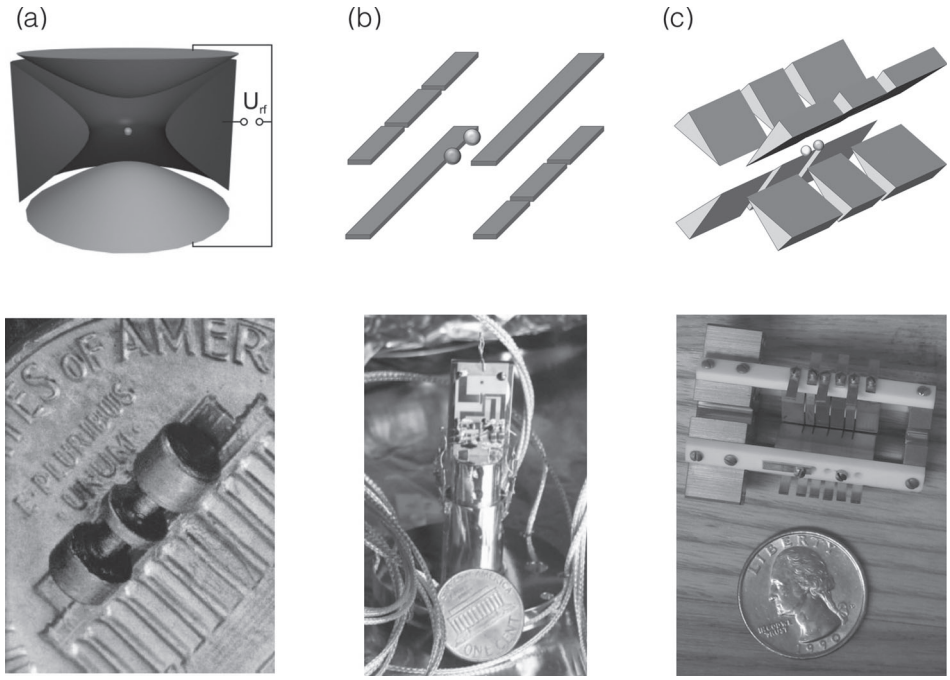

FIGURE 9.4 Examples of RF Paul ion trap geometries. (a) The spherical Paul trap used for the Hg+ frequency standard at NIST. The diagram is from Ludlow et al. (2015) and illustrates the cylindrically symmetric oscillating potential U_{RF} confining the Hg+ ion in red, which is applied between the ring and the end cap electrodes. (b) The linear chip Paul trap used for one of the two Al+ frequency standards at NIST, with the Be+ logic ion in orange and the Al+ clock ion in green. (c) The linear blade Paul trap used for the second Al+ frequency standard at NIST, with the Mg+ logic ion in yellow. All pictures of the traps are taken from the NIST image gallery, and the synergies associated with NIST's position within the US Department of Commerce are also apparent.

desirable clock properties such as small BBR coefficients and narrow clock transition linewidths, but which lack a convenient optical cycling transitions required for laser cooling and electron-shelving-based state read-out (Schmidt et al. 2005). An example is Al+, for which the $1S_0$ to $3P_0$ clock transition has an 8 mHz linewidth and an anomalously low BBR coefficient (see Table 9.1), but for which the strong $1S_0$ to $1P_1$ cycling transition is deep in the UV at 169 nm, and is therefore currently inaccessible. Quantum logic spectroscopy works by trapping a single clock ion such as Al+ with a "logic" ion in the same harmonic-trapping potential. The logic ion is chosen for its efficient cooling transitions and high-fidelity internal state read-out. Thanks to the strong coulomb interaction between the clock ion and the logic ion, Doppler and sideband cooling of the logic ion can be used to sympathetically cool the clock ion. In addition, after the clock ion has been probed with the clock laser, a two-qubit quantum gate can be applied to transfer the internal state of the clock ion into the logic ion to be read out (Schmidt et al. 2005). Figure 9.5 shows the outcome of a recent comparison between two Al+ clocks that make use of quantum logic spectroscopy, demonstrating a single-clock stability of $\sigma_y(\tau) = 2.8\times10^{-15}/\sqrt{\tau}$ (Chou, Hume, Koelemeij, Wineland & Rosenband 2010).

9.3.3.2 Ion Clock Systematics

The current generation ion clocks are primarily limited by the systematic effects discussed in Section 9.3.2. Second-order Doppler shifts arising from the micromotion and the harmonic, or "secular," motion of the ion in its tight trapping potential are particularly significant, but are mitigated by the remarkable levels of precision with which the motional states of a single ion can be characterized and controlled. A representative systematic evaluation for a Yb+ ion clock is shown in Table 9.2, published in Huntemann et al. (2016). The dominant sources of systematic uncertainty were the second-order Doppler shifts, the remaining blackbody shift, and the ac Stark shift from the clock laser itself. A total uncertainty of 3.2×10^{-18} was achieved by taking advantage of a second narrow linewidth transition in Yb+ with stronger coupling to magnetic and electric fields in order to evaluate the field-induced shifts of the clock transition, including the blackbody shift.

TABLE 9.2

Evaluated Systematic Shifts for a Yb+ Ion Clock at PTB

Effect	Shift (10^{-18})	Uncertainty (10^{-18})
Second-order Doppler shift	−3.7	2.1
BBR shift	−70.5	1.8
Probe light related shift	0	1.1
Second-order Zeeman shift	−40.4	0.6
Quadratic dc Stark shift	−1.2	0.6
Background-gas collisions	0	0.5
Servo error	0	0.5
Quadrupole shift	0	0.3
Total	−115.8	3.2

Source: All values are taken from Huntemann et al. (2016).

9.3.4 Neutral Atom Optical Lattice Clocks

In an optical lattice clock thousands of neutral atoms are confined in a trapping potential generated by the interference pattern of counter-propagating laser beams. The strong confinement provided by the lattice isolates the narrow internal optical clock transition from the motion of the atoms. Because they are neutrally charged, the atoms interact only weakly (Martin et al. 2013) and can all be probed simultaneously with the same probe laser, increasing the achievable N over ion clocks and thereby offering record-setting stabilities (Schioppo et al. 2017, Campbell et al. 2017). To date, absolute frequency measurements of optical lattice clocks with the alkaline-earth element strontium and the alkaline-earth-like elements ytterbium and mercury have been demonstrated. While the increased number of atoms and the use of an optical lattice results in additional systematic shifts that must be evaluated and controlled, optical lattice clocks have also recently demonstrated accuracies at the 10^{-18} level (Nicholson et al. 2015).

9.3.4.1 Optical Lattice Clock Operation

In a typical OLC, hot atoms are loaded from an oven source into the clock chamber through a "Zeeman slower," so that by the time they reach the chamber the atoms are near rest along the axis of the slower. Once inside the clock chamber,

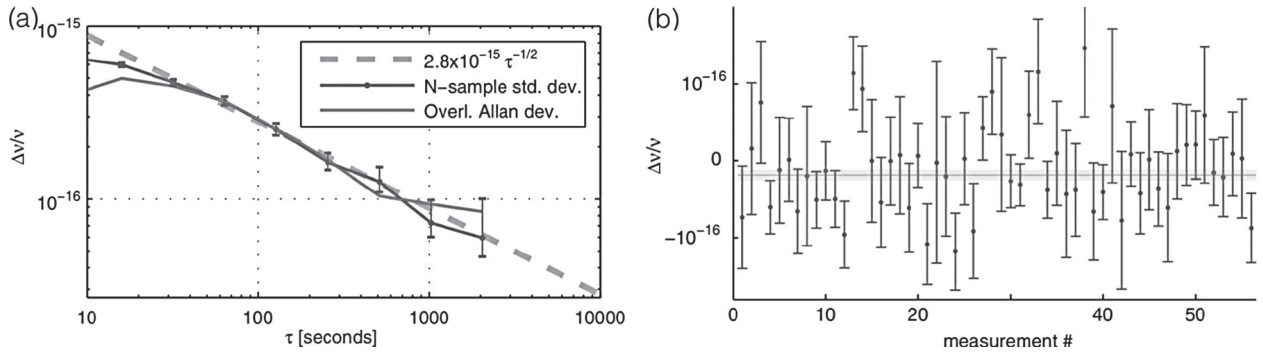

FIGURE 9.5 Comparison between two quantum logic ion optical clocks. (a) Fractional frequency uncertainty vs averaging period for a comparison between the two Al+ clocks at NIST. (b) Measurements of the fractional frequency difference between the two clocks Al+ (blue points). Error bars represent the statistical uncertainty. The horizontal line shows the weighted mean of the difference between the two clocks, -1.8×10^{-17}, and the shaded yellow bar the standard deviation of 7×10^{-18}. (Figures from Chou, Hume, Koelemeij, Wineland & Rosenband 2010.)

the atoms are captured and cooled in one or two stages of magneto-optical-traps (MOTs), a common atomic physics technique that combines 3D laser cooling with a conservative potential achieved using magnetic field gradients generated by anti-Helmholtz coils (Metcalf & Van der Straten 2007) (Figure 9.6).

After MOT cooling, the atoms are sufficiently cold and localized to be trapped by the optical dipole force in a one-dimensional optical lattice formed by a laser beam interfering with its counter-propagating retro-reflection. The importance of the strong optical confinement provided by the lattice is illustrated in the data shown in Figure 9.7b. When there is no axial trapping potential, (red diamonds), the clock transition has a Doppler-broadened linewidth due to the finite temperature of the atoms. As the axial trapping potential is increased, the motional sidebands become spectrally resolved, and the clock carrier transition at zero detuning narrows. In a deep lattice (blue squares) the clock is in the side-band-resolved and Lamb-Dicke regimes, and the finite temperature of the atoms has a negligible effect on the clock transition linewidth.

Unfortunately the trapping light also results in significant shifts of the internal structure of the atoms through the ac Stark effect, potentially leading to troublesome shifts of the clock transition that are dependent on both the lattice intensity and frequency. This can be partially circumvented by using a "magic wavelength" trap, where the frequency of the trapping light is carefully chosen such that the light-dependent frequency shifts of the two clock states cancel to first order. Nevertheless, as discussed in Section 9.3.4.2, the residual lattice shifts must be carefully evaluated.

Once the lattice has been ramped up, thousands of atoms at μK temperatures are confined in two-dimensional pancake-like optical potentials with depths of tens of μK (see Figure 9.7a), and they are ready to be probed on the narrow clock transition using the sequences described in Section 9.3.1 without suffering adverse effects from their finite temperature. Due to the shallow trapping depth, in optical lattice clocks the fluorescence measurements of the clock state populations typically heat the atoms out of the lattice, and new atoms must be cooled and loaded into the lattice for each measurement cycle.

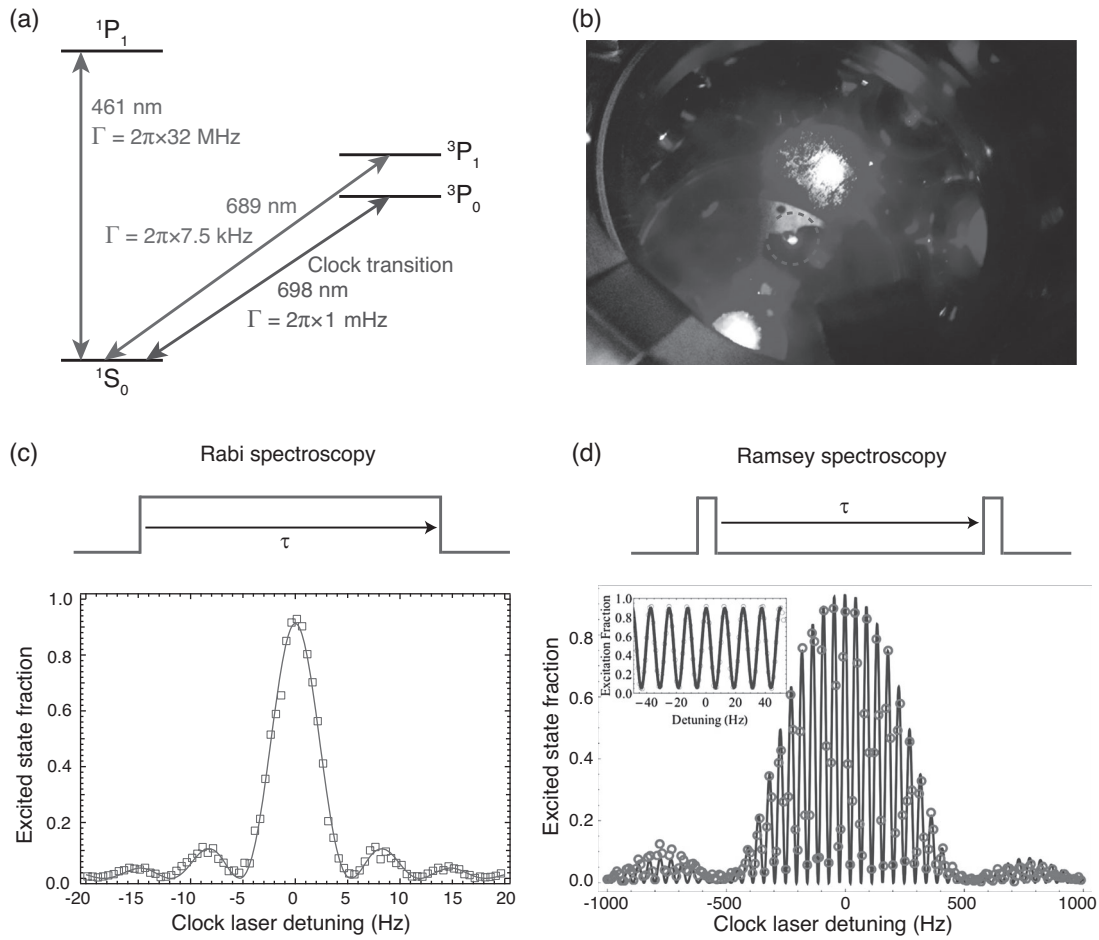

FIGURE 9.6 Standard strontium OLC operation. (a) A simplified level structure of 87Sr with the relevant cooling and clock transitions. (b) A picture of the 87Sr blue MOT in a strontium optical lattice clock in the Ye group at JILA. The 87Sr atoms are visible as a glowing blue ball in the centre of the red dashed circle. (c) A Rabi scan of the clock transition in the deep lattice regime, taken with the same strontium optical lattice clock. Here, the observed linewidth is a result of the Fourier limit for the applied 160 ms π-pulse. (d) The measured excitation fraction versus detuning for Ramsey spectroscopy where detuning is scanned over a larger range than the Rabi frequency. The inset shows the measured excitation fraction versus detuning using Ramsey spectroscopy for a π/2-pulse time of 750 μs and a free evolution time of 80 ms that is scanned ±50 Hz from resonance. (Figure from Refs. Martin 2013 and Bishof 2014.)

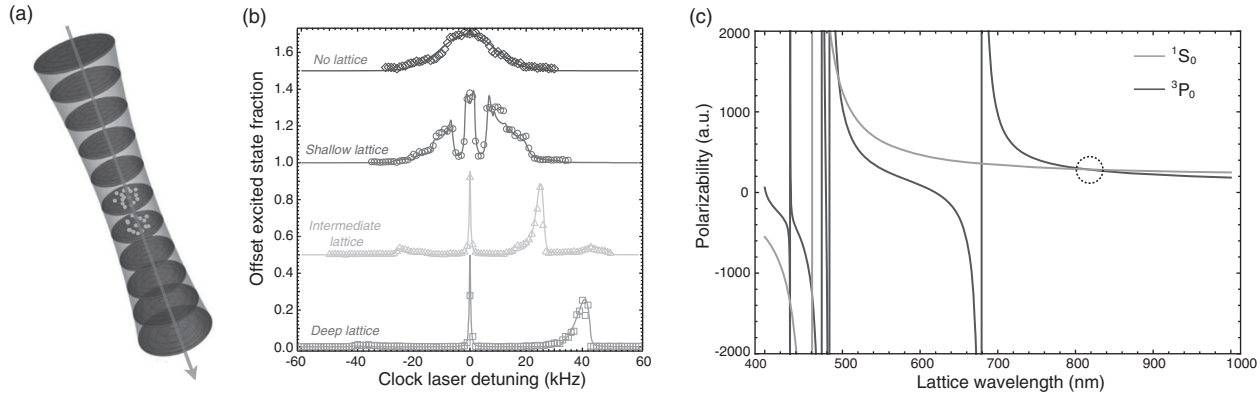

FIGURE 9.7 Strong confinement in an optical lattice. (a) A cartoon of atoms inside a 1D optical lattice, probed with a clock laser along the lattice axis. (b) Clock spectroscopy of a strontium optical lattice clock in the Ye group at JILA, published in Kolkowitz et al. (2017), showing the impact of the depth of the magic wavelength optical lattice on the 698-nm clock transition in a horizontal lattice. The axial motional sidebands of the lattice become well resolved from the narrow clock transition at zero detuning as the depth of the lattice is increased. The pronounced asymmetry between the red and blue sidebands illustrates that the atoms are primarily in the ground band on the lattice. (c) Polarizability curves for the two neutral strontium clocks states ($1S_0$ in blue, $3P_0$ in red). The "magic wavelength" at 813 nm is highlighted in the black dashed circle.

In Figure 9.8, a comparison between two ytterbium optical lattice clocks is shown, demonstrating a single-clock stability of $\sigma_y(\tau) = 3.2\times10^{-16}/\sqrt{\tau}$, and $\sigma_y = 1.6\times10^{-18}$ at 25000 s (Hinkley et al. 2013).

9.3.4.2 Optical Lattice Clock Systematics

A representative systematic evaluation for a strontium optical lattice clock is shown in Table 9.3. In addition to the systematics already discussed in Section 9.3.3.2, one of the unique systematics for optical lattice clocks is the ac Stark shift from the lattice light (Brown et al. 2017). While the lattice frequency and polarization are carefully selected to operate as close as possible to the "magic wavelength" condition, uncertainty in these parameters can result in a significant systematic shift. In the limit where the ac Stark shift depends only linearly on the lattice trap depth U_o, the full expression for the lattice frequency shift of the clock transition $\Delta\nu_{\text{lattice}}$ as a function of the lattice frequency f is given by

$$\Delta\nu_{\text{lattice}} = U_o\left\{\Delta\kappa_s(f) + \Delta\kappa_v(f)m_f\xi\vec{k}\cdot\vec{B} + [3m_f^2 - F(F+1)]\left(3\left|\vec{\varepsilon}\cdot\vec{B}\right|^2 - 1\right)\Delta\kappa_t(f)\right\} \quad (9.6)$$

where $\vec{k}$ is the lattice propagation vector, $\vec{\varepsilon}$ is the lattice polarization vector, ξ is the lattice polarization ellipticity (0 indicates linear polarization), $\vec{B}$ is the bias magnetic field direction,

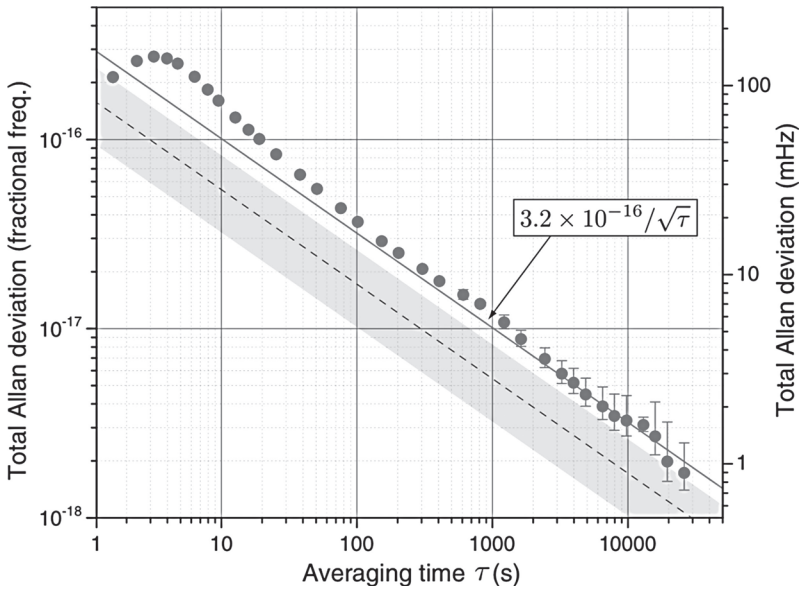

FIGURE 9.8 Comparison between two Yb optical lattice clocks. Extracted single-clock fractional frequency uncertainty and frequency uncertainty vs averaging time for a comparison between the two optical lattice clocks at NIST. The blue dashed line represents the estimated combined instability contributions from the Dick effect; the shaded region denotes uncertainty in these estimates. (This figure is from Hinkley et al. 2013 and is reprinted with permission from AAAS.)

TABLE 9.3

Evaluated Systematic Shifts for a Strontium Optical Lattice Clock at JILA

Effect	Shift (10^{-18})	Uncertainty (10^{-18})
Lattice ac Stark shift	–1.3	1.1
BBR static shift	–4562.1	0.3
BBR dynamic shift	–305.3	1.4
dc Stark shift	0	0.1
Probe ac Stark shift	0	0.0
First-order Zeeman shift	–0.2	0.2
Quadratic Zeeman shift	–51.7	0.3
Density shift	–3.5	0.4
Line-pulling+tunnelling	0	<0.1
Second-order Doppler shift	0	<0.1
Background gas collision shift	0	<0.6
Servo offset shift	–0.5	0.4
AOM phase chirp	0.6	0.4
Total	–4929.0	2.1

Source: All values are taken from Nicholson et al. (2015).

F is the total angular momentum quantum number, m_f is the hyperfine spin state, and $\Delta\kappa_s$, $\Delta\kappa_v$, and $\Delta\kappa_t$ are the differential scalar, vector, and tensor shift coefficients, respectively (Nicholson et al. 2015). The vector Stark shift can be doubly suppressed through a combination of linearly polarized lattice light with $\xi = 0$ and by aligning the lattice perpendicular to the magnetic field such that $\vec{k} \cdot \vec{B} = 0$. The "magic wavelength" is then the particular frequency f' for which the scalar and tensor shifts cancel and $\Delta\nu_{\text{lattice}} = 0$ for the operating conditions of the clock. Using this technique lattice Stark shift uncertainties at the 1.1×10^{-18} level have been demonstrated (Nicholson et al. 2015). At these levels of uncertainty the higher order nonlinear scaling of the ac Stark shift with lattice depth due to the atomic hyperpolarizability must also be accounted for (Brown et al. 2017), and reaching lower levels of uncertainty with optical lattice clocks will likely require new techniques to mitigate the ac Stark shift, as we discuss in Section 9.4.1.1.

Another important systematic shift in optical lattice clocks is the density shift due to collisional interactions between atoms occupying the same lattice site. These interactions not only introduce a significant frequency shift but also result in line-broadening that can limit the coherent interrogation times (Bloom et al. 2014). The loading of the lattice from the MOT results in a Poissonian probability distribution for the number of atoms on each site (Swallows et al. 2012). For each measurement sequence each lattice site therefore has a different density and a different corresponding collisional shift, leading to inhomogeneous broadening of the clock line, and to line pulling and corresponding systematic uncertainty. Until recently, the principle approach to this problem has been to decrease the density using the largest possible lattices and keeping the atom number low, and then to evaluate the density shift by interleaving measurements between high and low densities and performing a self-comparison (Bloom et al. 2014, Le Targat et al. 2013). However, as described in Section 9.4.1, the use of a Fermi-degenerate 3D optical lattice to greatly increase atomic density whilst effectively eliminating the onsite interaction shift has recently been demonstrated (Campbell et al. 2017). With single-site interactions controlled or eliminated, it is likely that the collective dipolar interactions between atoms on nearby lattice sites will now become significant (Bromley et al. 2016). This constant emergence of new, ever more complicated systematics is a common theme in optical clock research, and whilst it may seem vexing, it also offers exciting opportunities for new discoveries and clock applications, as we discuss in the following section.

9.4 Outlook and Future Directions

9.4.1 Next-Generation Clocks

In the prior sections of this chapter we have discussed a number of factors that currently limit the stability and accuracy of optical clocks. Fortunately, despite the fact that optical clocks are already operating at remarkable levels of precision, there are a number of emerging next-generation optical clock technologies that promise to enable further gains. Here we give a brief overview of some of these promising developments.

9.4.1.1 3D Optical Lattice Clocks

As described in Section 9.3.4, the current generation of optical lattice clocks makes use of 1D optical lattices, in which multiple neutral atoms are loaded into each pancake-shaped lattice site. The atoms are therefore in well-defined quantized motional states along the axis of the lattice, but their motion is thermal along the weakly confined transverse dimensions. The resulting collisional interactions between atoms occupying the same lattice sites give rise to an unfortunate trade-off between the atom number N and the coherent interrogation time and magnitude of the density shift, limiting both the stabilities and accuracies of these clocks. However, by adding additional lattice beams, strong confinement of clock atoms in two and even three dimensions has previously been achieved (Swallows et al. 2011, Akatsuka et al. 2010). It was recently demonstrated that the strong confinement provided by a 3D lattice clock results in spectrally well-resolved on-site interactions that eliminate line-broadening and line-pulling from collisional interactions (Campbell et al. 2017). Furthermore, the loading of a 3D optical lattice clock from a Fermi-degenerate gas offers the prospect of millions of atoms deterministically loaded into the lattice with unit filling factor, which each atom in a well-defined quantum state like an ion clock. When used for differential clock comparisons or in concert with new ultra-stable optical cavities, 3D lattice clocks will likely provide order of magnitude gains in clock stability. Furthermore, the introduction of high numerical aperture optical imaging of the lattice offers new possibilities for the characterization and control of systematics, as well as the single-shot measurement of Rabi lines and Ramsey fringes to characterize laser noise spectra (Marti et al. 2018). Of course, the evolution of optical lattice clock geometry is unlikely to stop here. The observation of Raman scattering out of the excited clock state due to the high-intensity 3D lattice beams (Campbell et al. 2017) has motivated new proposals for 3D "accordion lattices" formed

by beams at acute angles. These lattices will have large, tunable spacings between the lattice sites, enabling clock operation at low lattice intensities without the detrimental effects of tunnelling (Hutson et al. 2018).

9.4.1.2 Cryogenic Optical Clocks

As described in Section 9.3.2, one of the primary limiting systematic effects in both ion and optical lattice clocks is the shift due to BBR. To reach the 10−18 level of systematic uncertainty, optical clocks have already had to employ atoms with especially small blackbody coefficients (Chou, Hume, Koelemeij, Wineland & Rosenband 2010), the use of the most accurate thermometers available (Nicholson et al. 2015), or the use of an in-vacuum radiation shield (Beloy et al. 2014). However, the scaling of this shift with the temperature of the surrounding environment (T^4 for the static contribution and T^6 for the dynamic contribution,) means that by moving from atoms surrounded by 300 K ambient room temperature to the 4 K cryogenic temperatures achievable in a helium-based cryostat, this systematic can be suppressed by many orders of magnitude. This is difficult to implement because the atoms must be entirely enclosed by cryogenic radiation shields, as even a very small solid-angle opening to surfaces at warmer temperatures can result in large uncertainties (Ushijima et al. 2015). Despite the technical challenges, the first generation of cryogenic ion clocks and optical lattice clocks have already been realized (Ushijima et al. 2015, Rosenband et al. 2008).

9.4.1.3 Superradiant Optical Clocks

The challenges associated with building ever more stable passive optical cavities to reduce clock laser linewidths and mitigate the Dick effect (see Section 9.2.1) motivate the search for other approaches. One of the most promising alternatives is the development of an active optical frequency reference, in analogy to the hydrogen masers that act as active references in the microwave regime and offer excellent short-term stability to complement the long-term stability of microwave atomic clocks. The optical equivalent is a superradiant ultra-narrow linewidth laser, in which neutral atoms are placed inside an optical cavity tuned to resonance with a narrow atomic clock transition (Meiser et al. 2009, Bohnet et al. 2012). Atoms pumped into the excited clock state will then experience superradiant collective emission into the cavity mode, with the coherence of the light determined not by the cavity but by the atoms. The first demonstration of pulsed superradiant emission with an ultra-narrow optical clock transition was recently performed with strontium (Norcia et al. 2018). Efforts to extend these encouraging results to continuous wave (CW) superradiant emission are ongoing, with prospects for use both to enhance the performance of traditional optical clocks, and as a complementary optical clock technology with outstanding short-term stability.

9.4.1.4 Entangled Clocks

While equation (9.1) from Section 9.1.1 represents the quantum projection noise (QPN) limit to the stability of an optical clock with N independent atoms, it is in principle possible to further enhance the clock stability by placing the atoms in non-classical entangled states such as spin-squeezed states and maximally entangled Greenberger-Horne-Zeilinger states (Wineland et al. 1992, Leroux et al. 2010, Bohnet et al. 2014, Kessler et al. 201$\sqrt{4}$). This can push the stability of the clock below the QPN limit given by equation (4.8.1), which scales with $1/\sqrt{N}$, towards the ultimate Heisenberg limit allowed by quantum mechanics (Wineland et al. 1992), which scales with $1/N$. This is particularly attractive in light of the increased atom numbers promised by the 3D lattice clocks discussed in Section 9.4.1.1. However, in order to generate entanglement between the internal states of the atoms, a method for engineering strong, controllable atom–atom interactions is required. Proposed approaches include the use of high-finesse optical cavity to generate strong light-mediated atom–atom interactions (Norcia & Thompson 2016), or the use of Rydberg states to enhance the strength and length-scale of the atom–atom interactions (Gil et al. 2014, Kómár et al. 2016). Once entangled states have been generated they will be particularly sensitive to sources of decoherence including laser noise, and so they may prove to be most useful for clocks with small numbers of atoms such as ion clocks, or for differential clock comparisons in which the laser noise can be eliminated (Marti et al. 2018).

9.4.1.5 Exotic Atomic Clocks

While the optical atomic clocks described in this chapter are the most developed and widely adopted frequency standards, new kinds of exotic clocks are just beginning to emerge as next-generation optical clock candidates. For example, electronic transitions in highly charged ions (Safronova et al. 2014) and the intra-nuclear transition in 229Th (Campbell et al. 2012) have been proposed as promising clock transitions due to their insensitivity to external perturbations and their higher frequencies. With the recent demonstration of the trapping and sympathetic cooling of individual highly charged ions (Schmöger et al. 2015), there is now a zoo of highly charged ions and corresponding transitions to be explored spanning the entire periodic table. Furthermore, the prospects for enhanced sensitivity to variations in fundamental constants have motivated proposals for the use of clock transitions in highly charged ions and weakly bound molecules in searches for new physics (Safronova et al. 2014, Zelevinsky et al. 2008), as discussed in Section 9.4.2.

9.4.2 Emerging Applications of Optical Clocks

9.4.2.1 SI Unit Definitions, the World Clock, Navigation, and Geodesy

The most obvious application of optical clocks is to the definition and measurement of time and frequency. The SI second is currently defined with respect to the hyperfine transition of caesium. Because time can be defined more precisely than other units, in the new SI unit system currently being adopted, almost all other physical units are defined with respect to this definition of the second and fundamental constants. A worldwide collaboration of standard institutes and laboratories

operate the microwave atomic clocks that are averaged together to form the International Atomic Time that serves as the world clock. Optical clocks have already demonstrated accuracies surpassing caesium standards, and it seems clear that eventually an optical atomic transition will be adopted as the new primary definition of the second. However, for time being optical clocks are not yet sufficiently robust or widely available to warrant this switch. In the meantime, several optical transitions have been recognized as "secondary representations of the second," and optical clocks will soon contribute to steering the world clock (Ludlow et al. 2015).

Optical clocks will also likely begin to have a technological impact beyond timekeeping, with potential applications to navigation and geodesy. Microwave atomic clocks already play a central role in the Global Navigation Satellite Systems such as the Global Positioning System (GPS), networks of satellites which provide position and navigation information around the world. Although the positioning accuracy of the GPS is not presently limited by the stability of the vapour cell microwave atomic clocks in the satellites, these clocks require regular hourly corrections from the ground control stations in order for the network to remain synchronized and not accumulate significant errors. Adding additional space-based optical clock satellite nodes would improve GPS system integrity because the network would require less frequent ground-to-space based communications for clock correction and could potentially operate autonomously for days or weeks at a time (Ludlow et al. 2015).

As discussed in Section 9.3.2, the sensitivity of optical clock comparisons to changes in the gravitational potential presents a challenge for high-accuracy clock comparisons but also offers an opportunity to harness optical clocks for "relativistic geodesy." Once optical clock comparisons over long distances have reached the point where geodetic surveys are no longer sufficient to measure the changes in gravitational potential between optical clocks at their levels of relative accuracy, the clocks themselves will become the best tools for the job. Portable optical clocks could be compared locally, then moved to two distant locations and compared over a fibre or free-space optical link to determine their relative height, even between continents. Indeed, the first demonstrations of geodesy measurements between clocks connected over fibre links have already taken place (Takano et al. 2016, Lisdat et al. 2016).

9.4.2.2 Searches for Variations of Fundamental Constants, Dark Matter, and Gravitational Waves

As optical clocks continue to improve in accuracy, their sensitivity to signals of interest for fundamental physics research also grows. For example, because the energies of atomic clock transitions depend on fundamental constants such as the electron–proton mass ratio and the fine structure constant, comparisons between clock transitions that scale differently with these constants, such as comparisons between different atomic species, between microwave and optical clocks, or between two transitions in the same species with different character as in the Yb+ ion, can probe whether these fundamental constants are changing with time (Safronova et al. 2017). Long time-scale comparisons over many years have already placed constraints on slow variations (Huntemann et al. 2014), whilst short time-scale comparisons can search for faster coherent oscillations that might be induced by certain ultra-light dark-matter candidates (Arvanitaki et al. 2015).

Another promising approach for the future is to separate two identical space-based optical clocks over a large baseline and to compare their relative frequencies over an optical link. This type of detector would be sensitive to variations in fundamental constants as a function of position due to the motion of the satellites through a background dark-matter field (Arvanitaki et al. 2016), or to changes in the light travel time between the two clocks due to passing low-frequency gravitational waves (Kolkowitz et al. 2016). The sensitivity of this class of detector can be further enhanced using differential comparisons between the clocks that cancel sensitivity to laser noise, as well as measurement sequences that lock-in to specific frequencies (Kolkowitz et al. 2016).

9.4.2.3 Many-Body Quantum Physics

While the density shift in optical lattice clocks is a troublesome systematic that is typically minimized by operating at low densities, the many-body quantum physics underlying it has proven to be complex and rich (Martin et al. 2013). In addition, the inherent insensitivity to external perturbations and high degree of control demanded by high-accuracy optical clocks is ideal for the characterization of complex interactions and dynamics. As a result, precision clock spectroscopy is emerging as a powerful new tool for the study of exotic quantum systems. A wide range of interesting physics has already been observed, including SU(N) symmetry (Zhang et al. 2014), spin-orbit coupling (Kolkowitz et al. 2017, Livi et al. 2016), and interaction-induced spin-rephasing (Bromley et al. 2018, Norcia et al. 2017). The recent demonstration of a Fermi-degenerate 3D lattice clock (see Section 9.4.1.1) is certain to add access to additional phenomena, such as long-range dipolar interactions and many-body phase transitions.

REFERENCES

Akatsuka, T., Takamoto, M. & Katori, H. (2010), 'Three-dimensional optical lattice clock with bosonic Sr 88 atoms', *Physical Review A* **81**(2), 023402.

Arvanitaki, A., Graham, P. W., Hogan, J. M., Rajendran, S. & Van Tilburg, K. (2016), 'Search for light scalar dark matter with atomic gravitational wave detectors', *arXiv preprint arXiv:1606.04541*.

Arvanitaki, A., Huang, J. & Van Tilburg, K. (2015), 'Searching for dilaton dark matter with atomic clocks', *Physical Review D* **91**(1), 015015.

Beloy, K., Hinkley, N., Phillips, N. B., Sherman, J. A., Schioppo, M., Lehman, J., Feldman, A., Hanssen, L. M., Oates, C. W. & Ludlow, A. D. (2014), 'Atomic clock with 1×10^{-18} room-temperature blackbody Stark uncertainty', *Physical Review Letters* **113**(26), 260801.

Beloy, K., Zhang, X., McGrew, W., Hinkley, N., Yoon, T., Nicolodi, D., Fasano, R., Schäffer, S., Brown, R. & Ludlow, A. (2018), 'Faraday-shielded dc Stark-shift-free optical lattice clock', *Physical Review Letters* **120**(18), 183201.

Bishof, M. (2014), Understanding atomic interactions in an optical lattice clock and using them to study many-body physics, *PhD thesis*, University of Colorado at Boulder.

Bishof, M., Zhang, X., Martin, M. J. & Ye, J. (2013), 'Optical spectrum analyzer with quantum- limited noise floor', *Physical Review Letters* **111**(9), 093604.

Bloom, B. J., Nicholson, T. L., Williams, J. R., Campbell, S. L., Bishof, M., Zhang, X., Zhang, W., Bromley, S. L. & Ye, J. (2014), 'An optical lattice clock with accuracy and stability at the 10^{-18} level', *Nature* **506**(7486), 71–75.

Bohnet, J. G., Chen, Z., Weiner, J. M., Meiser, D., Holland, M. J. & Thompson, J. K. (2012), 'A steady-state superradiant laser with less than one intracavity photon', *Nature* **484**(7392), 78.

Bohnet, J. G., Cox, K. C., Norcia, M. A., Weiner, J. M., Chen, Z. & Thompson, J. K. (2014), 'Reduced spin measurement backaction for a phase sensitivity ten times beyond the standard quantum limit', *Nature Photonics* **8**(9), 731–736.

Bromley, S., Kolkowitz, S., Bothwell, T., Kedar, D., Safavi-Naini, A., Wall, M., Salomon, C., Rey, A. & Ye, J. (2018), 'Dynamics of interacting fermions under spin–orbit coupling in an optical lattice clock', *Nature Physics* 14(4), 399–404.

Bromley, S. L., Zhu, B., Bishof, M., Zhang, X., Bothwell, T., Schachenmayer, J., Nicholson, T. L., Kaiser, R., Yelin, S. F., Lukin, M. D., Rey, A. M. (2016), 'Collective atomic scattering and motional effects in a dense coherent medium', *Nature communications* **7**, 11039.

Brown, R., Phillips, N., Beloy, K., McGrew, W., Schioppo, M., Fasano, R., Milani, G., Zhang, X., Hinkley, N., Leopardi, H., Yoon, T. H. (2017), 'Hyperpolarizability and operational magic wavelength in an optical lattice clock', *arXiv preprint arXiv:1708.08829.*

Campbell, C. J., Radnaev, A. G., Kuzmich, A., Dzuba, V. A., Flambaum, V. V. & Derevianko, A. (2012), 'Single-ion nuclear clock for metrology at the 19th decimal place', *Physical Review Letters* **108**(12), 120802.

Campbell, G. K., Ludlow, A. D., Blatt, S., Thomsen, J. W., Martin, M. J., de Miranda, M. H., Zelevinsky, T., Boyd, M. M., Ye, J., Diddams, S. A., Heavner, T. P. (2008), 'The absolute frequency of the ^{87}Sr optical clock transition', *Metrologia* **45**(5), 539.

Campbell, S. L., Hutson, R., Marti, G., Goban, A., Oppong, N. D., McNally, R., Sonderhouse, L., Robinson, J., Zhang, W., Bloom, B., Ye, J. (2017), 'A Fermi-degenerate three-dimensional optical lattice clock', *Science* **358**(6359), 90–94.

Chou, C., Hume, D., Koelemeij, J., Wineland, D. & Rosenband, T. (2010), 'Frequency comparison of two high-accuracy Al^+ optical clocks', *Physical Review Letters* **104**, 070802.

Chou, C., Hume, D., Rosenband, T. & Wineland, D. (2010), 'Optical clocks and relativity', *Science* **329**(5999), 1630–1633.

Christensen, B. T., Henriksen, M. R., Schäffer, S. A., Westergaard, P. G., Tieri, D., Ye, J., Holland, M. J. & Thomsen, J. W. (2015), 'Nonlinear spectroscopy of Sr atoms in an optical cavity for laser stabilization', *Physical Review A* **92**(5), 053820.

Cole, G. D., Zhang, W., Martin, M. J., Ye, J. & Aspelmeyer, M. (2013), 'Tenfold reduction of Brownian noise in high-reflectivity optical coatings', *Nature Photonics* **7**(8), 644.

Cook, S., Rosenband, T. & Leibrandt, D. R. (2015), 'Laser-frequency stabilization based on steady- state spectral-hole burning in Eu^{3+}:Y_2SiO_5', *Physical Review Letters* **114**(25), 253902.

Cundiff, S. T. & Ye, J. (2003), 'Colloquium: Femtosecond optical frequency combs', *Reviews of Modern Physics* **75**(1), 325.

Diddams, S. A., Bergquist, J. C., Jefferts, S. R. & Oates, C. W. (2004), 'Standards of time and frequency at the outset of the 21st century', *Science* **306**(5700), 1318–1324.

Drever, R., Hall, J. L., Kowalski, F., Hough, J., Ford, G., Munley, A. & Ward, H. (1983), 'Laser phase and frequency stabilization using an optical resonator', *Applied Physics B* **31**(2), 97–105.

Gil, L., Mukherjee, R., Bridge, E., Jones, M. & Pohl, T. (2014), 'Spin squeezing in a Rydberg lattice clock', *Physical Review Letters* **112**(10), 103601.

Hinkley, N., Sherman, J. A., Phillips, N. B., Schioppo, M., Lemke, N. D., Beloy, K., Pizzocaro, M., Oates, C. W. & Ludlow, A. D. (2013), 'An atomic clock with 10^{-18} instability', *Science* **341**(6151), 1215–1218.

Hoyt, C., Barber, Z., Oates, C. W., Fortier, T., Diddams, S. & Hollberg, L. (2005), 'Observation and absolute frequency measurements of the $^1S_0$–$^3P_0$ optical clock transition in neutral ytterbium', *Physical Review Letters* **95**(8), 083003.

Huntemann, N., Lipphardt, B., Tamm, C., Gerginov, V., Weyers, S. & Peik, E. (2014), 'Improved limit on a temporal variation of m_p/m_e from comparisons of Yb^+ and Cs atomic clocks', *Physical Review Letters* **113**(21), 210802.

Huntemann, N., Sanner, C., Lipphardt, B., Tamm, C. & Peik, E. (2016), 'Single-ion atomic clock with 3×10^{-18} systematic uncertainty', *Physical Review Letters* **116**(6), 063001.

Hutson, R. et al. (2018), *In preparation*.

Ido, T. & Katori, H. (2003), 'Recoil-free spectroscopy of neutral Sr atoms in the Lamb-Dicke regime', *Physical Review Letters* **91**(5), 053001.

Jiang, Y., Ludlow, A., Lemke, N. D., Fox, R. W., Sherman, J. A., Ma, L.-S. & Oates, C. W. (2011), 'Making optical atomic clocks more stable with 10–16-level laser stabilization', *Nature Photonics* **5**(3), 158.

Kessler, E., M., Komar, P., Bishof, M., Jiang, L., Sorensen, A. S., Ye, J. & Lukin, M. D. (2014), 'Heisenberg-limited atom clocks based on entangled qubits', *Physical Review Letters* **112**, 190403.

Kessler, T., Hagemann, C., Grebing, C., Legero, T., Sterr, U., Riehle, F., Martin, M. J., Chen, L. & Ye, J. (2012), 'A sub-40-mHz-linewidth laser based on a silicon single-crystal optical cavity', *Nature Photonics* **6**(10), 687–692.

Kolkowitz, S., Bromley, S., Bothwell, T., Wall, M., Marti, G. E., Koller, A. P., Zhang, X., Rey, A. M. & Ye, J. (2017), 'Spin-orbit-coupled fermions in an optical lattice clock', *Nature* **542**(20811), 66–70.

Kolkowitz, S., Pikovski, I., Langellier, N., Lukin, M. D., Walsworth, R. L. & Ye, J. (2016), 'Gravi- tational wave detection with optical lattice atomic clocks', *Physical Review D* **94**(12), 124043.

Kómár, P., Topcu, T., Kessler, E., Derevianko, A., Vuletić, V., Ye, J. & Lukin, M. (2016), 'Quantum network of atom clocks: A possible implementation with neutral atoms', *Physical Review Letters* **117**(6), 060506.

Le Targat, R., Lorini, L., Le Coq, Y., Zawada, M., Guéna, J., Abgrall, M., Gurov, M., Rosenbusch, P., Rovera, D. G., Nagórny, B., Gartman, R., Westergaard, P. G., Tobar, M. E., Lours, M., Santarelli, G., Clairon, A., Bize, S., Laurent, P., Lemonde, P. & Lodewyck, J. (2013), 'Experimental realization of an optical second with strontium lattice clocks', *Nature Communications* **4**, 2109.

Leibfried, D., Blatt, R., Monroe, C. & Wineland, D. (2003), 'Quantum dynamics of single trapped ions', *Reviews of Modern Physics* **75**(1), 281.

Leroux, I. D., Schleier-Smith, M. H. & Vuletić, V. (2010), 'Implementation of cavity squeezing of a collective atomic spin', *Physical Review Letters* **104**, 073602.

Lisdat, C., Grosche, G., Quintin, N., Shi, C., Raupach, S., Grebing, C., Nicolodi, D., Stefani, F., Al-Masoudi, A., Dörscher, S., Häfner, S. (2016), 'A clock network for geodesy and fundamental science', *Nature communications* **7**, 12443.

Livi, L., Cappellini, G., Diem, M., Franchi, L., Clivati, C., Frittelli, M., Levi, F., Calonico, D., Catani, J., Inguscio, M., Fallani, L. (2016), 'Synthetic dimensions and spin-orbit coupling with an optical clock transition', *Physical Review Letters* **117**(22), 220401.

Ludlow, A. D., Boyd, M. M., Ye, J., Peik, E. & Schmidt, P. O. (2015), 'Optical atomic clocks', *Reviews of Modern Physics* **87**(2), 637.

Ludlow, A. D., Huang, X., Notcutt, M., Zanon-Willette, T., Foreman, S., Boyd, M., Blatt, S. & Ye, J. (2007), 'Compact, thermal-noise-limited optical cavity for diode laser stabilization at 1×10^{-15}', *Optics letters* **32**(6), 641–643.

Margolis, H., Huang, G., Barwood, G., Lea, S., Klein, H., Rowley, W., Gill, P. & Windeler, R. (2003), 'Absolute frequency measurement of the 674-nm $^{88}Sr^{+}$ clock transition using a femtosecond optical frequency comb', *Physical Review A* **67**(3), 032501.

Marti, G. E., Hutson, R. B., Goban, A., Campbell, S. L., Poli, N. & Ye, J. (2018), 'Imaging optical frequencies with 100 μ Hz precision and 1.1 μ m resolution', *Physical Review Letters* **120**(10), 103201.

Martin, M. J. (2013), Quantum metrology and many-body physics: pushing the frontier of the optical lattice clock, *PhD thesis*, University of Colorado at Boulder.

Martin, M. J., Bishof, M., Swallows, M. D., Zhang, X., Benko, C., von Stecher, J., Gorshkov, A. V., Rey, A. M. & Ye, J. (2013), 'A quantum many-body spin system in an optical lattice clock', *Science* **341**(6146), 632–636.

Matei, D. G., Legero, T., Häfner, S., Grebing, C., Weyrich, R., Zhang, W., Sonderhouse, L., Robinson, J. M., Ye, J., Riehle, F. & Sterr, U. (2017), '1.5 μm lasers with sub-10 mHz linewidth', *Physical Review Letters* **118**, 263202.

Meiser, D., Ye, J., Carlson, D. & Holland, M. (2009), 'Prospects for a millihertz-linewidth laser', Physical Review Letters **102**(16), 163601.

Metcalf, H. J. & Van der Straten, P. (2007), *Laser Cooling and Trapping of Neutral Atoms*, Wiley Online Library.

Millo, J., Magalhaes, D., Mandache, C., Le Coq, Y., English, E., Westergaard, P., Lodewyck, J., Bize, S., Lemonde, P. & Santarelli, G. (2009), 'Ultrastable lasers based on vibration insensitive cavities', *Physical Review A* **79**(5), 053829.

Nagourney, W., Sandberg, J. & Dehmelt, H. (1986), 'Shelved optical electron amplifier: Observation of quantum jumps', *Physical Review Letters* **56**(26), 2797.

Nazarova, T., Riehle, F. & Sterr, U. (2006), 'Vibration-insensitive reference cavity for an ultra- narrow-linewidth laser', *Applied Physics B* **83**(4), 531.

Nemitz, N., Ohkubo, T., Takamoto, M., Ushijima, I., Das, M., Ohmae, N. & Katori, H. (2016), 'Frequency ratio of Yb and Sr clocks with 5×10^{-17} uncertainty at 150 seconds averaging time', *Nature Photonics* **10**(4), 258.

Nicholson, T., Campbell, S., Hutson, R., Marti, G., Bloom, B., McNally, R., Zhang, W., Barrett, M., Safronova, M., Strouse, G., Tew, W. L. (2015), 'Systematic evaluation of an atomic clock at 2×10^{-18} total uncertainty', *Nature Communications* **6**, 1–8.

Norcia, M. A., Cline, J. R., Muniz, J. A., Robinson, J. M., Hutson, R. B., Goban, A., Marti, G. E., Ye, J. & Thompson, J. K. (2018), 'Frequency measurements of superradiance from the strontium clock transition', *Physical Review X* **8**(2), 021036.

Norcia, M. A., Lewis-Swan, R. J., Cline, J. R., Zhu, B., Rey, A. M. & Thompson, J. K. (2017), 'Cavity mediated collective spin exchange interactions in a strontium superradiant laser', *arXiv preprint arXiv:1711.03673*.

Norcia, M. A. & Thompson, J. K. (2016), 'Strong coupling on a forbidden transition in strontium and nondestructive atom counting', *Physical Review A* **93**(2), 023804.

Poli, N., Oates, C., Gill, P. & Tino, G. (2014), 'Optical atomic clocks', *arXiv preprint arXiv:1401.2378*.

Rosenband, T., Hume, D. B., Schmidt, P. O., Chou, C. W., Brusch, A., Lorini, L., Oskay, W. H., Drullinger, R. E., Fortier, T. M., Stalnaker, J. E., & Diddams, S. A. (2008), 'Frequency ratio of Al^{+} and Hg^{+} single-ion optical clocks; metrology at the 17th decimal place', *Science* **319**(5871), 1808–1812.

Safronova, M., Budker, D., DeMille, D., Kimball, D. F. J., Derevianko, A. & Clark, C. W. (2017), 'Search for new physics with atoms and molecules', *arXiv preprint arXiv:1710.01833*.

Safronova, M., Dzuba, V., Flambaum, V., Safronova, U., Porsev, S. & Kozlov, M. (2014), 'Highly charged ions for atomic clocks, quantum information, and search for α variation', *Physical Review Letters* **113**(3), 030801.

Santarelli, G., Audoin, C., Makdissi, A., Laurent, P., Dick, G. J. & Clairon, A. (1998), 'Frequency stability degradation of an oscillator slaved to a periodically interrogated atomic resonator', *IEEE Transactions on Ultrasonics, Ferroelectrics, and Frequency Control* **45**(4), 887–894.

Schioppo, M., Brown, R. C., McGrew, W. F., Hinkley, N., Fasano, R. J., Beloy, K., Yoon, T. H., Milani, G., Nicolodi, D., Sherman, J. A., Phillips, N. B., Oates, C. W. & Ludlow, A. D. (2017), 'Ultrastable optical clock with two cold-atom ensembles', *Nature Photonics* **11**(1), 48–52.

Schmidt, P. O., Rosenband, T., Langer, C., Itano, W. M., Bergquist, J. C. & Wineland, D. J. (2005), 'Spectroscopy using quantum logic', *Science* **309**(5735), 749–752.

Schmöger, L., Versolato, O., Schwarz, M., Kohnen, M., Windberger, A., Piest, B., Feuchtenbeiner, S., Pedregosa-Gutierrez, J., Leopold, T., Micke, P., & Hansen, A. K. (2015), 'Coulomb crystallization of highly charged ions', *Science* **347**(6227), 1233–1236.

Sherman, J. A., Lemke, N. D., Hinkley, N., Pizzocaro, M., Fox, R. W., Ludlow, A. D. & Oates, C. W. (2012), 'High-accuracy measurement of atomic polarizability in an optical lattice clock', *Physical Review Letters* **108**(15), 153002.

Stenger, J., Tamm, C., Haverkamp, N., Weyers, S. & Telle, H. R. (2001), 'Absolute frequency measurement of the 435.5-nm $^{171}Yb^{+}$-clock transition with a Kerr-lens mode-locked femtosecond laser', *Optics letters* **26**(20), 1589–1591.

Swallows, M. D., Bishof, M., Lin, Y., Blatt, S., Martin, M. J., Rey, A. M. & Ye, J. (2011), 'Suppression of collisional shifts in a strongly interacting lattice clock', *Science* **331**(6020), 1043–1046.

Swallows, M., Martin, M., Bishof, M., Benko, C., Lin, Y., Blatt, S., Rey, A. & Ye, J. (2012), 'Operating a ^{87}Sr optical lattice clock with high precision and at high density', *IEEE Transactions on Ultrasonics, Ferroelectrics, and Frequency Control* **3**(59), 416–425.

Takano, T., Takamoto, M., Ushijima, I., Ohmae, N., Akatsuka, T., Yamaguchi, A., Kuroishi, Y., Munekane, H., Miyahara, B. & Katori, H. (2016), 'Geopotential measurements with synchronously linked optical lattice clocks', *Nature Photonics* 10(10), 662–666.

Udem, T., Diddams, S. A., Vogel, K. R., Oates, C., Curtis, E., Lee, W., Itano, W., Drullinger, R., Bergquist, J. & Hollberg, L. (2001), 'Absolute frequency measurements of the Hg^{+} and Ca optical clock transitions with a femtosecond laser', *Physical Review Letters* **86**(22), 4996.

Ushijima, I., Takamoto, M., Das, M., Ohkubo, T. & Katori, H. (2015), 'Cryogenic optical lattice clocks', *Nature Photonics* **9**(3), 185.

Webster, S., Oxborrow, M., Pugla, S., Millo, J. & Gill, P. (2008), 'Thermal-noise-limited optical cavity', *Physical Review A* **77**(3), 033847.

Westergaard, P. G., Lodewyck, J. & Lemonde, P. (2010), 'Minimizing the Dick effect in an optical lattice clock', *IEEE Transactions on Ultrasonics, Ferroelectrics, and Frequency Control* **57**(3), 623–628.

Wineland, D. J., Bollinger, J. J., Itano, W. M., Moore, F. L. & Heinzen, D. J. (1992), 'Spin squeezing and reduced quantum noise in spectroscopy', *Physical Review A* **46**, R6797–R6800.

Yamanaka, K., Ohmae, N., Ushijima, I., Takamoto, M. & Katori, H. (2015), 'Frequency ratio of ^{199}Hg and ^{87}Sr optical lattice clocks beyond the SI limit', *Physical Review Letters* **114**(23), 230801.

Zelevinsky, T., Kotochigova, S. & Ye, J. (2008), 'Precision test of mass-ratio variations with lattice-confined ultracold molecules', *Physical Review Letters* **100**(4), 043201.

Zhang, W., Robinson, J., Sonderhouse, L., Oelker, E., Benko, C., Hall, J., Legero, T., Matei, D., Riehle, F., Sterr, U., & Ye, J. (2017), 'Ultrastable silicon cavity in a continuously operating closed-cycle cryostat at 4 k', *Physical review letters* **119**(24), 243601.

Zhang, X., Bishof, M., Bromley, S. L., Kraus, C. V., Safronova, M. S., Zoller, P., Rey, A. M. & Ye, J. (2014), 'Spectroscopic observation of SU(N)-symmetric interactions in Sr orbital magnetism', *Science* **345**(6203), 1467–1473.

FURTHER READING

Interested readers looking for a more comprehensive and detailed discussion of optical clocks are encouraged to read these two excellent recent review articles:

Ludlow, D., Boyd, M. M., Ye, J., Peik, E., & Schmidt, P. O. (2015), 'Optical atomic clocks,' *Reviews of Modern Physics* 87(2), 637.

Poli, N., Oates, C., Gill, P., & Tino, G. (2014), 'Optical atomic clocks,' *arXiv preprint arXiv:1401.2378*.